K. F. Cheung

Assistant Professor,
Department of Ocean Engineering,
University of Hawaii at Manoa,
2540 Dole Street, Holmes Hall 402,
Honolulu, HI 96822

M. Isaacson

Professor,
Department of Civil Engineering,
University of British Columbia,
Vancouver, B.C., Canada V6T 1Z4

J. W. Lee

Associate Professor,
Department of Ocean Civil Engineering,
Korea Maritime University,
Pusan 606-791, Korea

Wave Diffraction Around Three-Dimensional Bodies in a Current

The effects of a collinear current on the diffraction of regular waves around three-dimensional surface-piercing bodies are examined. With the current speed assumed to be small, the boundary-value problem is separated into a steady current problem with a rigid wall condition applied at the still water level and a linear wave propagation problem in the resulting current field. The boundary conditions of the wave propagation problem are satisfied by a time-stepping procedure and the field solution is obtained by an integral equation method. Free surface profiles, runup, and wave forces are described for a vertical circular cylinder in combined waves and a current. The current is shown to affect significantly the steady drift force and runup predictions. Comparisons of the computed wave forces are made with a previous numerical solution involving a semi-immersed sphere in deep water, and indicate good agreement.

1 Introduction

Accurate predictions of wave effects on large structures in combined waves and currents are of practical importance in the design and operation of these structures in the natural environment. By considering a reference frame fixed to the current, this problem is equivalent to the drift motions or maneuvers of a large offshore structure or ship in waves. If the current speed or the forward speed of a drifting structure is small, the effects of flow separation are generally unimportant and the problem can be described adequately by potential theory.

Restricting the applications to fully submerged bodies, the flow field can be separated into a steady wave component associated with the current and a propagating component associated with the radiated and diffracted waves (e.g., Grue and Palm, 1985; Wu and Eatock Taylor, 1987; and Wu, 1991). If the current speed is small, the steady wave system generated in the vicinity of the body is insignificant. The free surface boundary conditions for the steady current problem can be reduced to a rigid-wall condition, and the method can be applied more generally to surface-piercing bodies. Based on the condition of infinitely deep water, Zhao and Faltinsen (1988) and Wu and Eatock Taylor (1990) provided numerical solutions for two-dimensional surface-piercing bodies, and Nossen et al. (1991) applied the method in three dimensions. Grue and Biberg (1993) generalized the method for finite water depth applications. Other applications were made by Grue and Palm (1993) to calculate the wave-drift damping coefficients and by Ertekin et al. (1994) to study the interaction of waves with a steady intake-pipe flow.

All of the aforementioned solutions for the wave-current interaction problem have been developed in the frequency domain. Isaacson and Cheung (1993) provided a time-domain solution for wave diffraction and radiation in the presence of a current. Their treatment of the free surface boundary conditions is based on a slow current, but does not require the assumption of infinitely deep water. The numerical procedure has been found to be stable and robust. The present paper considers an extension of their method to three dimensions. Applications of the method are made to the diffraction of regular waves around a surface-piercing circular cylinder and a semi-immersed sphere.

2 Theoretical Formulation

With reference to Fig. 1, the boundary-value problem is defined with a right-handed Cartesian coordinate system (x, y, z), in which x and y are measured horizontally and z is measured vertically upward from the still water surface S_o. The body located at the center of the domain is rigid and fixed, and its surface below the still water level is indicated by S_b. The seabed is assumed impermeable and horizontal in the plane $z = -d$. The infinite domain is truncated by a vertical control surface S_c located at a sufficiently far distance from the body. The incident waves and the uniform current are collinear in the x-z plane.

The fluid is assumed to be incompressible and inviscid, and the flow irrotational. The flow field is described by a velocity potential ϕ satisfying the Laplace equation

$$\nabla^2\phi = 0 \qquad (1)$$

Since a linear solution is sought, the potential can be expressed as a sum of individual components proportional to the current speed and wave height, respectively,

$$\phi = \phi_u + \phi_b + \phi_w + \phi_s \qquad (2)$$

in which

$$\phi_u = Ux \qquad (3)$$

represents the potential of the uniform current, and U is the current speed. The potential ϕ_b is the steady disturbance to the uniform current by the body; and ϕ_w and ϕ_s indicate, respectively, the incident and scattered wave potentials.

Since the current speed is assumed to be small, the steady component of the free surface elevation is negligible. The free surface elevation is therefore expressed as a sum of the incident and scattered wave components as

$$\eta = \eta_w + \eta_s \qquad (4)$$

In the presence of a uniform current, linear wave theory gives the incident potential and free surface elevation, respectively, as

$$\phi_w = \frac{2\pi A}{kT}\frac{\cosh\,[k(z + d)]}{\sinh\,(kd)}\sin\,(kx - \omega_c t) \qquad (5)$$

$$\eta_w = A\cos\,(kx - \omega_c t) \qquad (6)$$

in which $\omega_c = \omega + kU$ is the angular frequency of the incident waves relative to a fixed reference frame and t denotes time. In
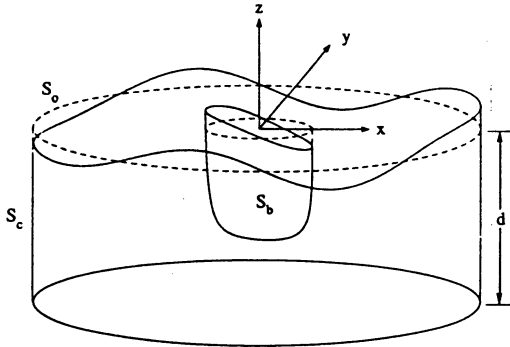
Fig. 1 Definition sketch of mathematical model

Eqs. (5) and (6), A is the incident wave amplitude, T is the wave period relative to the uniform current, k is the wave number of the incident waves, and $\omega = 2\pi/T$ is the angular frequency relative to the uniform current.

With the uniform current and incident wave potentials specified, separate boundary-value problems for ϕ_b and ϕ_s may be developed by a perturbation expansion using small parameters σ and ϵ, relating to the current speed and wave height, respectively, (Isaacson and Cheung, 1993).

2.1 Steady Current Problem. The boundary-value problem for ϕ_b describing the modification of the uniform current by the body can be obtained by collecting terms to order ϵ^0, and retaining terms to order σ. The boundary conditions applied on the seabed and body surface are, respectively, given by

$$\frac{\partial \phi_b}{\partial z} = 0 \quad \text{at} \quad z = -d \quad (7)$$

$$\frac{\partial \phi_b}{\partial n} = -\frac{\partial \phi_u}{\partial n} = -Un_x \quad \text{on} \quad S_b \quad (8)$$

where n is distance in the direction of the unit normal vector $\mathbf{n} = (n_x, n_y, n_z)$ directed outward from the fluid region. Since the current speed is small and second-order terms in σ are ignored, the kinematic free surface boundary condition is reduced to a rigid-wall condition

$$\frac{\partial \phi_b}{\partial z} = 0 \quad \text{on} \quad S_o \quad (9)$$

The dynamic free surface boundary condition shows that the corresponding free surface elevation is second order in σ, and is not considered. Since the disturbance caused by the body is localized, it is required that the effects of ϕ_b vanish at large distance from the body. For bodies of simple geometry, a closed-form solution can be obtained by a number of standard methods, including mapping techniques. For bodies of arbitrary shape, a numerical solution may be obtained by an integral equation method.

2.2 Wave Propagation Problem. The boundary-value problem for the scattered potential ϕ_s may be established by collecting terms of order ϵ and retaining terms of up to order σ. The boundary conditions on the seabed and body surface are given, respectively, by

$$\frac{\partial \phi_s}{\partial z} = 0 \quad \text{at} \quad z = -d \quad (10)$$

$$\frac{\partial \phi_s}{\partial n} = -\frac{\partial \phi_w}{\partial n} \quad \text{on} \quad S_b \quad (11)$$

Due to the presence of the current, the linear kinematic and dynamic free surface boundary conditions are modified, respectively, to

$$\frac{\partial \phi_s}{\partial z} - \frac{\partial \eta_s}{\partial t} - U\frac{\partial \eta_s}{\partial x} = \left(\frac{\partial \eta_w}{\partial x} + \frac{\partial \eta_s}{\partial x}\right)\frac{\partial \phi_b}{\partial x}$$

$$+ \left(\frac{\partial \eta_w}{\partial y} + \frac{\partial \eta_s}{\partial y}\right)\frac{\partial \phi_b}{\partial y} - (\eta_w + \eta_s)\frac{\partial^2 \phi_b}{\partial z^2} \quad \text{on} \quad S_o \quad (12)$$

$$\frac{\partial \phi_s}{\partial t} + g\eta_s + U\frac{\partial \phi_s}{\partial x} = -\left(\frac{\partial \phi_w}{\partial x} + \frac{\partial \phi_s}{\partial x}\right)\frac{\partial \phi_b}{\partial x}$$

$$- \left(\frac{\partial \phi_w}{\partial y} + \frac{\partial \phi_s}{\partial y}\right)\frac{\partial \phi_b}{\partial y} \quad \text{on} \quad S_o \quad (13)$$

where g is the acceleration due to gravity. It should be noted that both the incident and scattered waves are modified by the local current field near the body as accounted for by the right-hand sides of Eqs. (12) and (13).

Due to the steady disturbance to the uniform current, the dispersion relation in the vicinity of the body is quite complicated. Far away from the body, the effects of ϕ_b vanish, and the celerity of the scattered waves varies with the azimuthal angle, depending on the angle between the scattered wave propagation and the current direction. The radiation condition is extended to account for the spatially dependent celerity

$$\frac{\partial \phi_s}{\partial t} + c\frac{\partial \phi_s}{\partial n} = 0 \quad \text{on} \quad S_c \quad (14)$$

where c is a locally determined celerity of the outgoing waves on the control surface.

This radiation condition was originally developed for two-dimensional hyperbolic flows (Orlanski, 1976). It has been applied to the second-order and full nonlinear wave diffraction problems in three dimensions (e.g., Isaacson and Cheung, 1992; and Yang and Ertekin, 1992), and to wave-current interaction problems in two dimensions (Isaacson and Cheung, 1993). In these studies, the radiation condition has been shown to be effective in reducing reflection from the control surface, and thereby minimizes the effects of the artificial boundary on the numerical solutions.

2.3 Integral Equation. The solution to the boundary-value problem of the scattered potential may be obtained by the application of an integral equation involving a Green function G

$$\phi_s(\mathbf{x}) = \frac{1}{2\pi}\int_S \left[G(\mathbf{x}, \xi)\frac{\partial \phi_s}{\partial n} - \phi_s(\mathbf{x})\frac{\partial G}{\partial n}(\mathbf{x}, \xi) \right] dS \quad (15)$$

where ξ represents a point on the surface S over which the integration is performed, and n is measured from ξ. The surface S would comprise of the body surface, the still water surface, the seabed, and a control surface. With the seabed horizontal and the flow symmetric about the x-axis, it is more efficient to exclude the seabed from S and to choose a Green function that accounts for the double symmetry about the x-axis and the seabed. This is

$$G(\mathbf{x}, \xi) = \sum_{k=1}^{4} \frac{1}{|\xi_k - \mathbf{x}|} \quad (16)$$

where ξ_k are the source points in the four quadrants of the doubly symmetric configuration (see Isaacson and Cheung, 1992).

2.4 Summary of Numerical Procedure. The numerical procedure described in Isaacson and Cheung (1992, 1993) can be applied directly to the foregoing formulation, and only a brief summary is provided here. The integral equation, Eq. (15), is solved by a numerical procedure in which the boundaries S_b, S_c, and S_o are discretized into finite numbers of planar quadrilateral facets. The corresponding values of ϕ_s and $\partial \phi_s / \partial n$ are taken as constant over each facet and applied at the centroid. Equation (15) is then reduced to a system of simultaneous equations. Since the coefficients of the simultaneous equations are functions of geometry and discretization only, the solution to the system of equations is required only once and the numerical model can be applied to different incident wave and current conditions.

The input vector to the system of equations consists of the normal derivative of the scattered potential on the body surface, which is known from the body surface boundary condition, as well as the potential on the control surface and the still water surface, which may be obtained by a time-stepping procedure applied to the corresponding boundary conditions. Initial conditions at $t = 0$ correspond to an undisturbed regular wave train riding on a uniform current in the computational domain and the body has no effects on the flow. The body surface boundary conditions (Eqs. (8) and (11)) are imposed gradually through the use of a modulation function and a steady-state solution in the vicinity of the body is developed after the first wave cycle.

2.5 Hydrodynamic Forces. With the current and wave potentials evaluated, the pressure in the fluid may be determined by the Bernoulli equation. The wave forces on the body can be determined by carrying out an integration of the pressure over the instantaneous wetted body surface. However, the pressure integration can be expanded about the still water level to give an integral over the body surface below the still water level S_b and an integral defined at the still waterline contour w_o. Collecting terms of order ϵ, the first-order oscillatory force is given by

$$\mathbf{F} = -\rho \int_{S_b} \left[\left(\frac{\partial \phi_w}{\partial t} + \frac{\partial \phi_s}{\partial t} \right) + \nabla(\phi_u + \phi_b) \right. $$
$$\left. \times \nabla(\phi_w + \phi_s) \right] \mathbf{n}' \, dS \quad (17)$$

in which $\mathbf{n}' = (n_x, n_y, n_z, yn_z - zn_y, zn_x - xn_z, xn_y - yn_x)$, and ρ is the water density. The force vector $\mathbf{F} = (F_x, F_y, F_z, M_x, M_y, M_z)$ represents the three components of wave forces and moments in the three translational and rotational directions, respectively. It should be noted that the second term of Eq. (17) derives from the velocity-squared term in the Bernoulli equation.

By collecting terms of order ϵ^2, the second-order steady force can be obtained from the solution of the first-order boundary value problem as

$$\mathbf{F} = -\frac{1}{2} \rho \left\langle \int_{S_b} |\nabla(\phi_w + \phi_s)|^2 \mathbf{n}' \, dS \right\rangle$$
$$+ \frac{1}{2} \rho g \left\langle \int_{w_o} (\eta_w + \eta_s)^2 \mathbf{n}' \, dw \right\rangle \quad (18)$$

where $\langle \rangle$ denotes a time average and w indicates distance along the still waterline contour. The second integral in Eq. (18) accounts for the steady wave force due to the fluctuation of the free surface around the body.

3 Results and Discussion

To illustrate the numerical model and to compare with a previous theoretical solution, applications are made to a bottom-
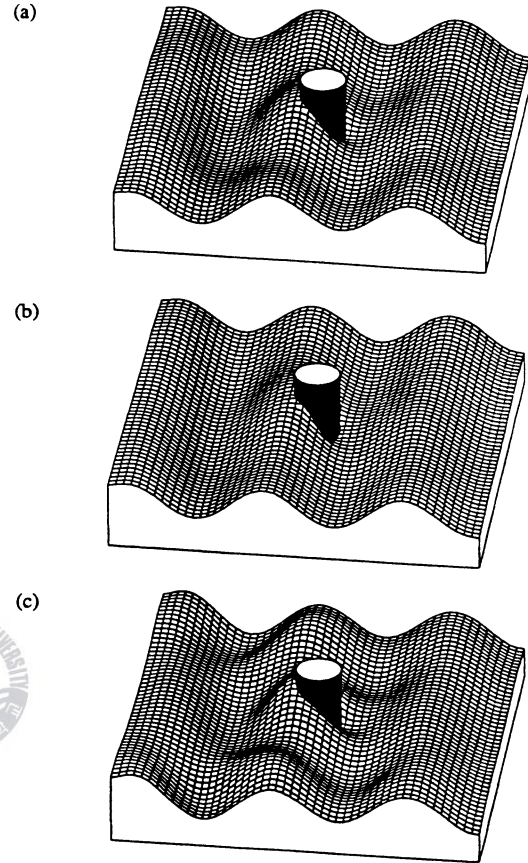

(a)

(b)

(c)

Fig. 2 Views of free surface profile around a circular cylinder for $ka = 1$ and $d/a = 1$; (a) $U/\sqrt{ga} = 0$, (b) $U/\sqrt{ga} = -0.1$, (c) $U/\sqrt{ga} = 0.1$

mounted, surface-piercing circular cylinder in finite water depth and a semi-immersed sphere in infinitely deep water. For these configurations, the closed-form solutions for the potential ϕ_b describing the steady disturbance to the uniform current by the bodies are known and are utilized in the numerical solution. The current speed is expressed in dimensionless form as the Froude number $U/\sqrt{ga}$, where a denotes the radius of the cylinder or the sphere. Since collinear waves and currents are considered, a negative value of the Froude number indicates a current in the negative x direction.

3.1 Free Surface Profiles. Let θ denote the azimuthal angle measured horizontally from the positive x-axis. The free surface profiles around a circular cylinder at the instants when the free surface elevation is maximum at $\theta/\pi = 1$ are shown in Fig. 2 for different values of the Froude number. The wave conditions correspond to $ka = 1$ and $d/a = 1$, and the incident waves propagate from left to right in the figures. Comparing to the case when $U/\sqrt{ga} = 0$ in Fig. 2(a), it is observed that the wave field in Fig. 2(b) is scattered to a lesser extent when the incident waves propagate in the opposite direction of the uniform current. In Fig. 2(c), the incident waves propagate in the same direction of the current and the scattered waves are more visible and their amplitudes are higher.

The propagation of the waves is modified more significantly by the current. Despite identical incident wavelengths in each
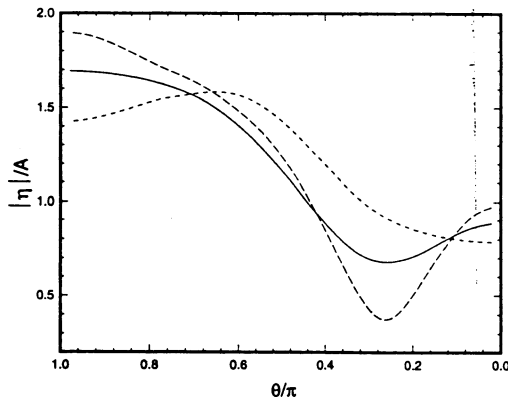
Fig. 3 Runup as a function of azimuthal angle around a circular cylinder for $ka = 1$ and $d/a = 1$; ——, $U/\sqrt{ga} = 0$; - - - -, $U/\sqrt{ga} = -0.1$; - - -, $U/\sqrt{ga} = 0.1$

of Figs. 2(a) to (c), the encounter frequency is different in each case owing to the presence of the current. On the surface of the cylinder, the current speed ranges from zero to $2U$, and both the incident and scattered wave fields are modified. Far away from the cylinder, the steady flow field approaches that of a uniform current. The scattered waves in the direction of the uniform current would have longer lengths and lower heights, and propagate at higher speeds. On the other hand, the scattered waves which propagate in the opposite direction of the current would have shorter lengths, higher heights, and lower speeds.

3.2 Runup. The runup around a circular cylinder for the conditions of $ka = 1$ and $d/a = 1$ is plotted in Fig. 3 as a function of the azimuthal angle. The solution corresponding to $U/\sqrt{ga} = 0$ is also shown in the figure to provide a reference for comparison. The runup is normalized with respect to the incident wave amplitude. Although the effects of the current on the runup vary depending on the azimuthal angle, the range of runup along the cylinder perimeter increases with the Froude number. When $U/\sqrt{ga} = -0.1$, the amplitudes of the scattered waves decrease at the front of the cylinder and the location of the maximum runup shifts from the front to the side. Figure 4
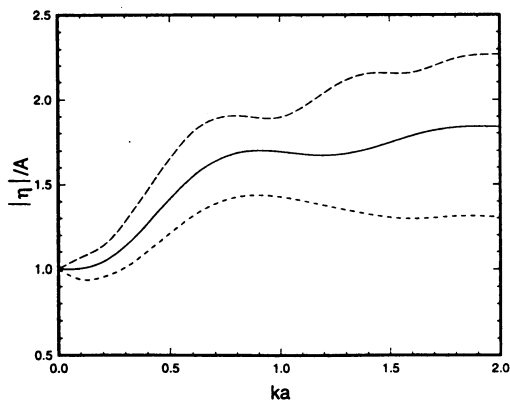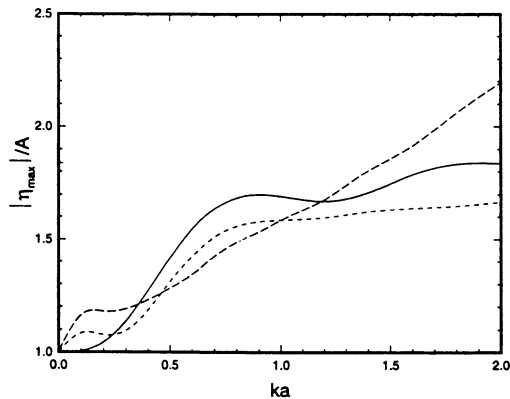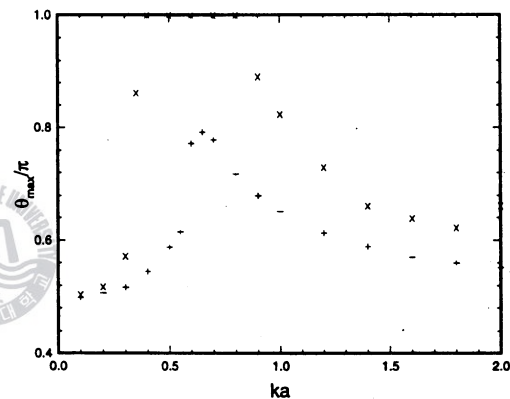

Fig. 4 Runup on a circular cylinder at $\theta/\pi = 1$ as a function of ka for $d/a = 1$ (see caption of Fig. 3 for legend)


(a) Maximum runup

(b) Location of maximum

Fig. 5 Maximum runup and location of maximum on a circular cylinder as functions of ka for $d/a = 1$. ——, $U/\sqrt{ga} = 0$; - - - -, ×, $U/\sqrt{ga} = -0.05$; - - -, +, $U/\sqrt{ga} = -0.1$.

shows the runup on a circular cylinder at $\theta/\pi = 1$ as a function of ka for $d/a = 1$. Due to increase in the scattered wave amplitude, the runup at $\theta/\pi = 1$ always increases with the Froude number.

For negative values of the Froude number, the maximum runup and its location on a circular cylinder are plotted, respectively, in Figs. 5(a) and (b) as functions of ka for $d/a = 1$. The runup when $U/\sqrt{ga} = 0$ is also shown for comparison. It is noted from Fig. 5(a) that the maximum runup around a circular cylinder does not necessarily decrease with a current in the opposite direction of the incident waves. In Fig. 5(b), the location of the maximum runup shifts from the front to the side of the cylinder for most of the wave and current conditions considered. While the variation of the maximum runup with ka is gradual and continuous, the location of the maximum shifts abruptly when $U/\sqrt{ga} = -0.05$ and $ka \approx 0.35$. Under these conditions, the runup on the upwave side of the cylinder is nearly uniform.

For the ranges of parameters considered, the runup and its variation along the cylinder perimeter exhibit nonlinear relations with U.

3.3 First-Order Oscillatory Forces. The amplitudes of the first-order oscillatory force and moment on a circular cylinder for different values of the Froude number are plotted as
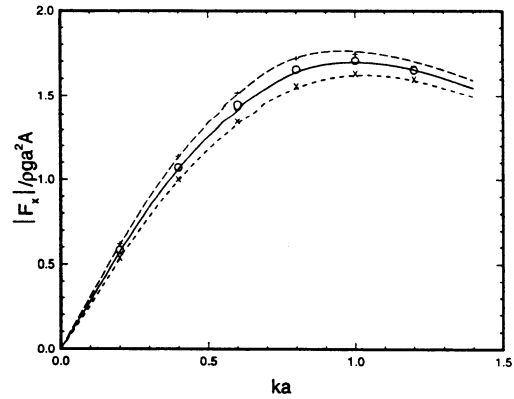
(a) Force

(a) x component
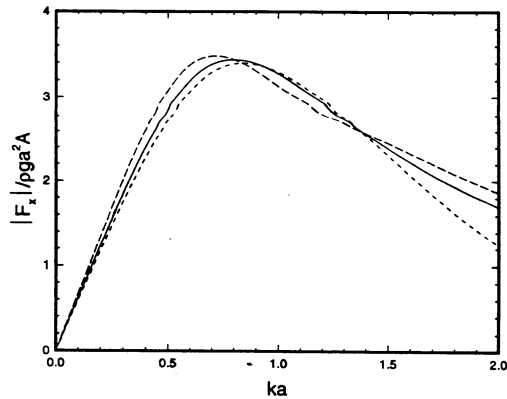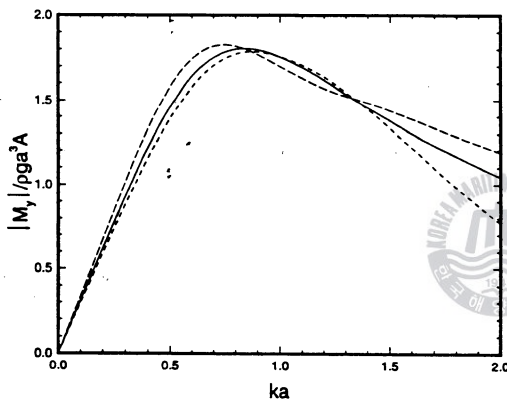
(b) Moment

(b) z component

Fig. 6 Amplitudes of the first-order oscillatory force and moment on a circular cylinder as functions of ka for $d/a = 1$ (see caption of Fig. 3 for legend)
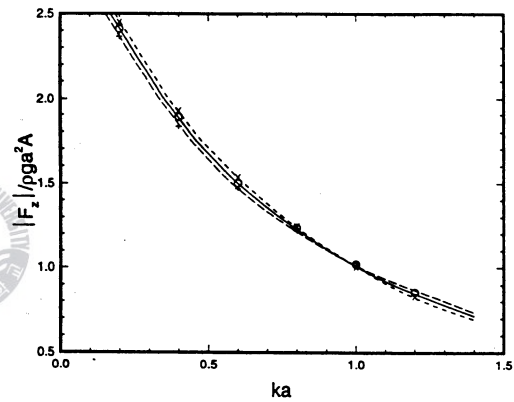
Fig. 7 Amplitude of the first-order oscillatory force on a semi-immersed sphere as a function of ka in deep water. Present study: ——, $U/\sqrt{ga} = 0$; - - - - -, $U/\sqrt{ga} = -0.04$; – – –, $U/\sqrt{ga} = 0.04$. Nossen et al. (1991): $\bigcirc$, $U/\sqrt{ga} = 0$; ×, $U/\sqrt{ga} = -0.04$; +, $U/\sqrt{ga} = 0.04$.

functions of ka in Figs. 6a and (b), respectively. It is noted that the amplitudes of the first-order oscillatory force and moment do not necessarily increase with the Froude number. In particular, the presence of a current in the direction of wave propagation decreases the force and moment predictions near $ka = 1$. In general, the effects of the current on the force and moment amplitudes are found to be nonlinear and are more significant for large values of ka.

To verify the present model, Figs. 7(a) and (b) show the comparisons between the computed amplitudes of the first-order oscillatory forces in the x and z directions with those of Nossen et al. (1991) for a semi-immersed sphere in infinitely deep water. The numerical solution of Nossen et al. was calculated using 200 facets on one-half of the body surface. To maintain a consistent resolution of the grid in terms of the wavelength, 250 to 490 facets were used in the calculation of the present results. The comparisons indicate good agreement. Based on an inspection of the numerical solution, the computed wave force amplitudes in both directions are generally found to be linear functions of the current speed.

3.4 Second-Order Steady Drift Forces. The second-order steady drift force on a circular cylinder, which is calculated on the basis of the first-order solution, is plotted as a function of ka for $d/a = 1$ in Fig. 8. It is noted that for the ranges of
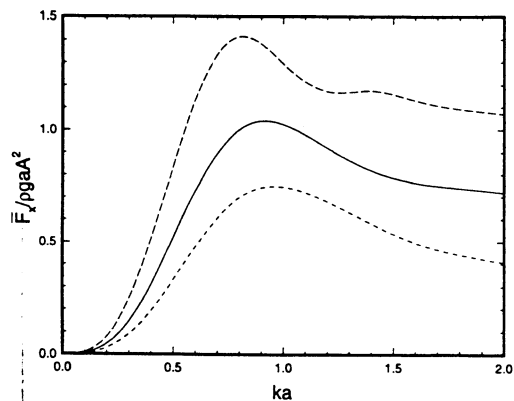

Fig. 8 Second-order drift force on a circular cylinder as a function of ka for $d/a = 1$ (see caption of Fig. 3 for legend)
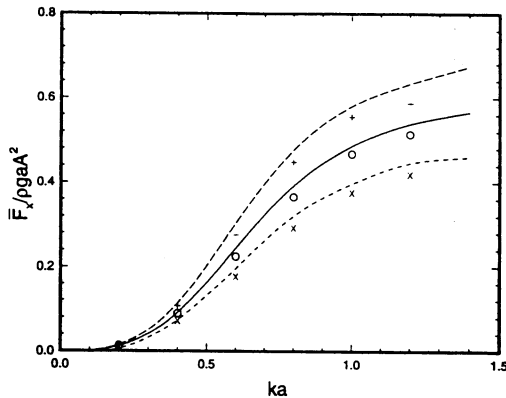
Fig. 9 Second-order drift force on a semi-immersed sphere as a function of ka in deep water (see caption of Fig. 7 for legend)

frequency and current speed considered, the second-order steady force varies nonlinearly with U. For the case of a semi-immersed sphere in deep water, the comparison between the computed second-order drift force and that of Nossen et al. (1991) is shown in Fig. 9. The present model gives slightly higher predictions compared to Nossen et al.'s numerical solution. It is expected that the discrepancy between the two numerical solutions is primarily due to the use of different number of facets to model the body, as discussed in Section 3.3.

For both bodies, the effects of the current on the second-order steady drift force are found to be more pronounced compared to the first-order forces, and the magnitude of the steady drift force always increases with the Froude number. This is primarily due to the effects of the current on the water surface elevation around the body, which in turn modifies the steady drift force prediction. As a result, the predicted low-frequency response of a floating structure would be modified significantly if forward speed effects are included in the computation of the drift force or the wave drift damping coefficient.

4 Conclusion

A time-domain method has been developed to treat the interactions between regular waves and a collinear current with large surface-piercing bodies of arbitrary shape in three dimensions. The present approach has been applied to wave diffraction for a bottom-mounted surface-piercing circular cylinder in finite water depth. The free surface profiles, runup, first-order oscilla-

tory and second-order steady forces are examined. The present numerical model is verified by comparing the computed forces with previous numerical results involving a semi-immersed sphere in deep water.

The results illustrate the importance of current or forward speed effects on a large offshore structure in waves and also the linear and nonlinear effects of the current on the solution. The numerical solution for the vertical cylinder is found to be a nonlinear function of the Froude number, while the solution for the semi-immersed sphere in deep water is shown to be a linear function of the Froude number. For the range of parameters considered, the presence of a current has been found to have significant effects on the runup and second-order steady force, whereas the first-order forces are affected to a lesser extent.

Acknowledgment

References

Ertekin, R. C., Liu, Y. Z., and Padmanabhan, B., 1994, "Interaction of Incoming Waves With a Steady Intake-Pipe Flow," ASME JOURNAL OF OFFSHORE MECHANICS AND ARCTIC ENGINEERING, Vol. 116, pp. 214–220.

Grue, J., and Palm, E., 1985, "Wave Radiation and Wave Diffraction From a Submerged Body in a Uniform Current," *Journal of Fluid Mechanics*, Vol. 151, pp. 257–278.

Grue, J., and Palm, E., 1993, "The Mean Drift Force and Yaw Moment on Marine Structures in Waves and Current," *Journal of Fluid Mechanics*, Vol. 250, pp. 121–142.

Grue, J., and Biberg, D., 1993, "Wave Forces on Marine Structures With Small Speed in Water of Restricted Depth," *Applied Ocean Research*, Vol. 15, No. 2, pp. 121–135.

Isaacson, M., and Cheung, K. F., 1992, "Second-Order Wave Diffraction in Three Dimensions," ASCE *Journal of Waterway, Port, Coastal and Ocean Engineering*, Vol. 118, No. 5, pp. 496–516.

Isaacson, M., and Cheung, K. F., 1993, "Time-Domain Solution for Wave-Current Interactions With a Two-Dimensional Body," *Applied Ocean Research*, Vol. 15, No. 1, pp. 39–52.

Nossen, J., Grue, J., and Palm, E., 1991, "Wave Forces on Three-Dimensional Floating Bodies With Small Forward Speed," *Journal of Fluid Mechanics*, Vol. 227, pp. 135–160.

Orlanski, I., 1976, "A Simple Boundary Condition for Unbounded Hyperbolic Flows," *Journal of Computational Physics*, Vol. 21, pp. 251–269.

Wu, G. X., and Eatock Taylor, R., 1987, "Hydrodynamic Forces on Submerged Oscillating Cylinders at Forward Speed," *Proceedings of Royal Society of London*, Series A, Vol. 414, pp. 149–170.

Wu, G. X., and Eatock Taylor, R., 1990, "The Hydrodynamic Force on an Oscillating Ship With Low Forward Speed," *Journal of Fluid Mechanics*, Vol. 211, pp. 333–353.

Wu, G. X., 1991, "Hydrodynamic Forces on a Submerged Cylinder Advancing in Water Waves of Finite Depth," *Journal of Fluid Mechanics*, Vol. 224, pp. 645–659.

Yang, C., and Ertekin, R. C., 1992, "Numerical Simulation of Nonlinear Wave Diffraction by a Vertical Cylinder," ASME JOURNAL OF OFFSHORE MECHANICS AND ARCTIC ENGINEERING, Vol. 114, pp. 36–44.

Zhao, R., and Faltinsen, O. M., 1988, "Interaction Between Waves and Current on a Two-Dimensional Body in the Free Surface," *Applied Ocean Research*, Vol. 10, No. 2, pp. 87–99.